Geotech Geol Eng (2024) 42:5003–5019
https://doi.org/10.1007/s10706-024-02826-0

ORIGINAL PAPER

Elastic Solutions of Circular Foundations Under Combined Loading

Pengpeng He · **Jesús González-Hurtado** · **Tim Newson**

Received: 7 December 2023 / Accepted: 9 May 2024 / Published online: 30 May 2024

Abstract The design of shallow foundations for wind turbines is typically governed by serviceability and fatigue limit states. To estimate the deformations of shallow foundations under working loads, existing design standards generally employ analytical uncoupled isotropic elastic solutions based on idealized soil conditions. However, many natural soil deposits exhibit some degree of stiffness anisotropy due to their deposition and complex stress history. This study has investigated coupled elastic stiffness coefficients for circular shallow foundations founded on cross-anisotropic soils under combined VHMT loadings (vertical, horizontal, moment and torsional) using finite element analysis. A three-parameter anisotropic soil model was applied to the problem. The study extensively explores the effects of soil stiffness non-homogeneity (i.e. linear increase of elastic modulus with depth) and foundation embedment on the foundation stiffness coefficients. Fitted expressions of these stiffness coefficients were also derived. In addition, a practical application using the proposed stiffness coefficients was presented to demonstrate the effects of soil stiffness anisotropy on the responses of a typical large wind turbine shallow foundation.

Keywords Wind turbine · Circular foundation · Foundation stiffness coefficient · Cross-anisotropy · Gibson soil

P. He
School of Science and Engineering, University of Dundee, Dundee, UK
e-mail: phe001@dundee.ac.uk

J. González-Hurtado · T. Newson (✉)
Geotechnical Research Centre, Department of Civil and Environmental Engineering, Western University, London, ON, Canada
e-mail: tnewson@eng.uwo.ca

J. González-Hurtado
e-mail: jgonza23@uwo.ca; jesus.gonzalez-hurtado@wsp.com

Present Address:
J. González-Hurtado
WSP Canada Inc, 1931 Robertson Road, Ottawa, ON, Canada

1 Introduction

Estimation of the serviceability limit state of shallow foundations under working loads can be of great significance (Buragadda and Orekanti 2023; Poulos 2023). This is particularly important for large onshore and offshore structures, such as wind turbines (WTs) and oil and gas platforms. The majority of large shallow WT foundations are circular or close to circular in form. These shallow foundations are generally subjected to combined loadings: vertical loads due to the self-weight of the structure (V), horizontal loads (H) caused by environmental conditions, overturning moments (M)

due to the horizontal loading and structural height, and torsional loads (T) induced by wind and structural effects. For serviceability limit states, the linear elastic behavior of the soil under normal working loads is often assumed. The rocking stiffness of WT foundations in particular is considered to be a critical design parameter, since it controls the location of the center of gravity with respect to the turbine foundation (Lang 2012).

Available analytical solutions for estimating the elastic response of surface-based rigid circular footings are based on theories that assume homogeneous elastic half-spaces subjected to uniaxial vertical, horizontal, moment and torsional loads. Various solutions can be found in the literature, e.g. Spence (1968), Gerrard and Harrison (1970), Poulos and Davies (1974) and Reissner and Sagoci (1944):

$$K_V = \frac{4\ln(3-4\mu)}{1-2\mu} \quad (1)$$

$$K_{HH} = \frac{8}{2-\mu} \quad (2)$$

$$K_{MM} = \frac{8}{3(1-\mu)} \quad (3)$$

$$K_T = \frac{16}{3} \quad (4)$$

where K_V, K_{HH}, K_{MM} and K_T are vertical, horizontal, moment and torsional elastic stiffness coefficients; and μ is the soil Poisson's ratio. Kausel et al. (1978) proposed approximate solutions for embedded circular foundations. Bell (1991) extended this concept to incorporate the cross-coupling effect between horizontal and rocking behavior in a matrix form:

$$\begin{bmatrix} \frac{V}{GR^2} \\ \frac{H}{GR^2} \\ \frac{M}{GR^3} \end{bmatrix} = \begin{bmatrix} K_V & 0 & 0 \\ 0 & K_{HH} & K_{HM} \\ 0 & K_{MH} & K_{MM} \end{bmatrix} \cdot \begin{bmatrix} u_V/R \\ u_H/R \\ \theta_M \end{bmatrix} \quad (5)$$

where u_V, u_H and θ_M are the vertical, horizontal and rotational deformations; G is the soil shear modulus; and R is the foundation radius. K_{MH} and K_{HM} are equal, representing the cross-coupling between the horizontal and rotational degrees of freedom. Note that torsion was not addressed by this study.

Stiffness coefficients have been found to depend on the soil Poisson's ratio, foundation embedment depth, foundation geometry, and embedment conditions. Doherty and Deeks (2003) further developed coupled VHM foundation stiffness coefficients considering both foundation embedment and soil non-homogeneity. However, the solutions of Bell (1991) and Doherty and Deeks (2003) are only applicable for isotropic soil conditions. In addition, despite the availability of coupled solutions (e.g. Gazetas 1991), uncoupled foundation stiffness methods still predominate in most guidelines for shallow foundation design, such as DNV (2016) and ISO (2016).

It is widely recognized that many natural soils are anisotropic or at least transversely isotropic (cross-anisotropic) due to their deposition and complex stress history (e.g. Zarei and Soltani-Jigheh 2021; Singh et al. 2024). It has been reported that stiffness anisotropy has a considerable impact on both short- and long-term ground movements predicted by tunnel excavation (Simpson et al. 1996; Franzius 2003). Burland et al. (1977) and Korobova et al. (2019) also showed that soil stiffness anisotropy significantly impacts foundation responses and should not be ignored. In practice, it is often assumed that elastic soil properties remain consistent regardless of direction. However, González-Hurtado (2019) demonstrated that this can lead to unconservative foundation design in terms of serviceability limit states. Gazetas (1981) analytically investigated the vertical, horizontal and rocking responses of surface strip foundations on cross-anisotropic soils. However, due to analytical complexities, the foundation stiffness cannot be explicitly given, rendering it less accessible for practical applications. In addition, the effect of soil stiffness anisotropy on foundation stiffness has not been examined.

To address this issue, this paper aims to derive explicit expressions of coupled foundation stiffness for circular foundations under combined VHMT loads, while accounting for the influence of soil stiffness anisotropy. A three-parameter cross-anisotropic model is first introduced to characterize the elastic soil behavior. Foundation stiffness coefficients, accounting for the effects of foundation embedment, soil stiffness non-homogeneity, and anisotropy, are then estimated using finite element (FE) analysis. In addition, a typical wind turbine shallow foundation is analysed to demonstrate the application of the derived foundation stiffness approach.

2 Cross-anisotropic soil stiffness model

As reported previously (Graham and Houlsby 1983; Grammatikopoulou et al. 2014), both granular soils and clays exhibit stiffness anisotropy characterized by cross-anisotropic elasticity. The relationship between the increments of effective stress and strain for a cross-anisotropic soil can be described by (Lings et al. 2000):

$$\begin{bmatrix} \delta\varepsilon_{xx} \\ \delta\varepsilon_{yy} \\ \delta\varepsilon_{zz} \\ \delta\gamma_{yz} \\ \delta\gamma_{zx} \\ \delta\gamma_{xy} \end{bmatrix} = \begin{bmatrix} \frac{1}{E_h} & -\frac{\mu_{hh}}{E_h} & -\frac{\mu_{vh}}{E_v} & \cdot & \cdot & \cdot \\ -\frac{\mu_{hh}}{E_h} & \frac{1}{E_h} & -\frac{\mu_{vh}}{E_v} & \cdot & \cdot & \cdot \\ -\frac{\mu_{vh}}{E_v} & -\frac{\mu_{vh}}{E_v} & \frac{1}{E_v} & \cdot & \cdot & \cdot \\ \cdot & \cdot & \cdot & \frac{1}{G_{vh}} & \cdot & \cdot \\ \cdot & \cdot & \cdot & \cdot & \frac{1}{G_{vh}} & \cdot \\ \cdot & \cdot & \cdot & \cdot & \cdot & \frac{1}{G_{hh}} \end{bmatrix} \cdot \begin{bmatrix} \delta\sigma'_{xx} \\ \delta\sigma'_{yy} \\ \delta\sigma'_{zz} \\ \delta\tau'_{yz} \\ \delta\tau'_{zx} \\ \delta\tau'_{xy} \end{bmatrix} \tag{6}$$

The subscripts in Eq. (6) follow the convention adopted by Pickering (1970). The stresses and strains are referred to three Cartesian axes, with x and y being the horizontal axis and z being the vertical axis of symmetry. Love (1892) showed that only five independent parameters are required to fully describe a cross-anisotropic elastic soil: Young's modulus in the horizontal direction, E_h; Young's modulus in the vertical direction, E_v; Poisson's ratio for horizontal strain due to vertical strain, μ_{vh}; Poisson's ratio for horizontal strain due to horizontal strain, μ_{hh}; and shear modulus in the vertical plane, G_{hv} ($G_{hv}=G_{vh}$). The remaining parameters can be related to these five parameters using:

$$G_{hh} = \frac{E_h}{2\left(1+\mu_{hh}\right)} \tag{7}$$

$$\frac{\mu_{hv}}{E_h} = \frac{\mu_{vh}}{E_v} \tag{8}$$

Equation (7) assumes that the horizontal plane is a plane of isotropy, and thermodynamic considerations require Eq. (8) to ensure the symmetry of the elastic compliance matrix.

Since thermodynamic considerations require positive strain energy of an elastic material, certain bounds on the five independent parameters also need to be satisfied. Pickering (1970) demonstrated that E_h, E_v and G_{hv} must always be positive, and inequalities (9) and (10) should also be satisfied. Raymond (1970) has showed that G_{hv} is constrained by inequality (11).

$$-1 < \mu_{hh} < 1 \tag{9}$$

$$\frac{E_v}{E_h}\left(1-\mu_{hh}\right) - 2\mu_{vh}^2 \geq 0 \tag{10}$$

$$G_{hv} \leq \frac{E_v}{2\mu_{vh}\left(1+\mu_{hh}\right) + 2\sqrt{\left(\frac{E_v}{E_h}\right)\left(1-\mu_{hh}^2\right)\left(1-\frac{E_h}{E_v}\mu_{vh}^2\right)}} \tag{11}$$

Graham and Houlsby (1983) proposed a simplified cross-anisotropic model, consisting of only three independent parameters: (i) modified Young's modulus: $E^* = E_v$; (ii) anisotropy factor: $\alpha = \sqrt{E_h/E_v}$; and modified Poisson's ratio: $\mu^* = \mu_{hh}$.

All of the five cross-anisotropic elastic parameters can thus be computed using these three parameters:

$$\begin{gathered} E_v = E^*; E_h = \alpha^2 E^* \\ G_{vh} = G_{hv} = \frac{\alpha E^*}{2(1+\mu^*)}; G_{hh} = \frac{\alpha^2 E^*}{2(1+\mu^*)} \\ \mu_{hh} = \mu^*; \mu_{vh} = \frac{\mu^*}{\alpha}; \mu_{hv} = \alpha\mu^* \end{gathered} \tag{12}$$

Substituting Eq. (12) into (10) yields $-1 < \mu^* = \mu_{hh} \leq 0.5$; therefore, 0.5 is an upper bound of μ_{hh} in this model.

As a special case of drained soil conditions, the undrained soil condition can be accommodated by mapping the drained parameters to undrained parameters. According to Ratananikom et al. (2013) and Lings (2001), the undrained Young's modulus and shear modulus of the three-parameter model can be expressed by Eq. (13), while Eqs. (7) and (8) remain applicable.

$$\begin{gathered} E_v^u = E^*\left[\frac{4\alpha\mu^* + 2\mu^* - 2 - \alpha^2}{2(\mu^*+1)(2\mu^*-1)}\right] \\ E_h^u = \alpha^2 E^*\left[\frac{4\alpha\mu^* + 2\mu^* - 2 - \alpha^2}{2\alpha\mu^*(\mu^*+1) + \left(\mu^{*2}-1\right)\left(\alpha^2+1\right)}\right] \\ G_{hh}^u = G_{hh}; G_{hv}^u = G_{hv} \end{gathered} \tag{13}$$

Following Bell (1991), the stiffness of a circular foundation on a cross-anisotropic soil under combined VHMT loads can be expressed in a matrix form as:

$$\begin{bmatrix} \frac{V}{G_{hv}R^2} \\ \frac{H}{G_{hv}R^2} \\ \frac{M}{G_{hv}R^3} \\ \frac{T}{G_{hv}R^3} \end{bmatrix} = \begin{bmatrix} K_V & 0 & 0 & 0 \\ 0 & K_{HH} & K_{HM} & 0 \\ 0 & K_{MH} & K_{MM} & 0 \\ 0 & 0 & 0 & K_T \end{bmatrix} \cdot \begin{bmatrix} u_V/R \\ u_H/R \\ \theta_M \\ \theta_T \end{bmatrix} \tag{14}$$

3 Finite element analysis

3.1 Material models and sign conventions

In this study, all of the finite element analyses were conducted using the software ABAQUS (Dassault Systèmes 2016), employing the full Newton's method to numerically solve equilibrium equations. The soil was modelled as a cross-anisotropic linear elastic material characterized by the three-parameter model (Eq. (12)), with isotropy as a special case (i.e. $\alpha^2=1$). As suggested by Lings (2001), Nishimura (2014) and Yimsiri and Soga (2011), the anisotropic ratio α^2 typically ranges from 0 to 2. Therefore, $\alpha^2=0.2$, 0.4, 0.6, 1.0, 1.5, and 2.0 were used in this study to cover most soils of practical interest. Given that context, the typical range of μ^* is $-1<\mu^*\leq 0.5$, μ^* was taken as 0, 0.1, 0.2, 0.3, 0.4, and 0.49.

The diameter (D) and thickness (t) of the foundation were taken as $D=19$ m and $t=3$ m, representing typical dimensions for current large wind turbines in North America. The effect of the foundation embedment (d) was studied by varying the embedment ratios from 0 to 0.16 (i.e. $d/D=0$, 0.03, 0.06, 0.09, 0.12, and 0.16), following the approach of González-Hurtado (2019). Since most natural deep soil deposits exhibit an increase of elastic stiffness with depth (Doherty and Deeks 2003; Rowe and Booker 1981), the soil was also modelled as a non-homogeneous layer with linearly increasing elastic modulus with depth (Gibson 1967). Different gradients (k) for the soil stiffness increase were considered for β (where $\beta=kD/E_{v0}$ is the normalized Gibson factor) varying from 0 to 0.40, corresponding to $k=0$, 1.0, 2.0, 3.0, 4.0 and 5.0 MPa/m, aligning with the studies of Gibson (1967) and Rowe and Booker (1981). $E_{v0}=237$ MPa was used in the analysis. Figure 1 shows the homogeneous and non-homogeneous soil profiles adopted herein. Cases of surface foundations on Gibson soils and embedded foundations in homogeneous soils were separately considered to investigate the effects of soil non-homogeneity and foundation embedment. Each case included 36 sub-cases (i.e. six values of $\alpha^2\times$six values of μ^*). The foundation was assumed to be a rigid body, with a load reference point (LRP) attached to the center of the foundation base to apply prescribed displacements or loads.

The base contact between the foundation and the soil was set as a rough condition (no horizontal movement of the soil nodes at the soil-anchor interface), implemented using the penalty method in ABAQUS (2016). For embedded foundations, a reduced friction coefficient (i.e. partially rough interface) for side and top interfaces is always recommended due to installation or in-service loading processes (Gourvenec and Mana 2011). In this analysis, smooth sides and top of the embedded foundations were assumed for conservative estimations. The foundation was also allowed to separate from the soil at zero normal contact stress at the interfaces. The sign conventions for the loads are illustrated in Fig. 1, where the horizontal and moment loads were considered to be in the same plane.

3.2 Geometry and mesh

A cylinder with finite dimensions was used to simulate the half-space soil. To minimize the effect of

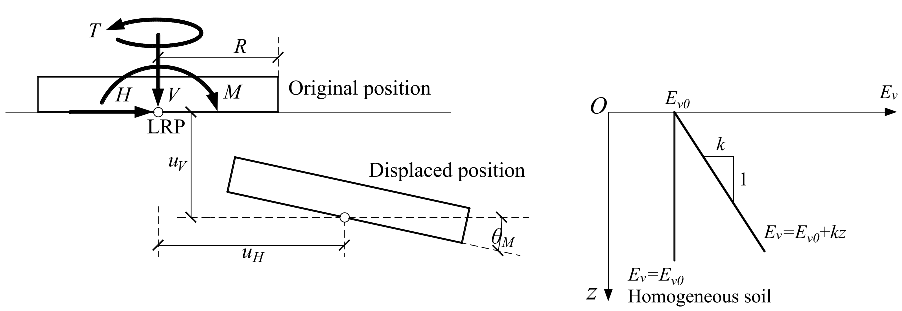

Fig. 1 Sign conventions and homogeneous and non-homogeneous soil profiles

boundaries on the numerical results, the size of the soil domain should be suffiently large (Maleki and Nabizadeh 2021; Maleki and Mir Mohammad Hosseini 2022; Maleki et al. 2023). In this part of the study, five model domain widths, L, (i.e. $L = 5D$, $10D$, $20D$, $50D$, and $100D$) were taken to examine boundary effects. These dimensions represent the horizontal distance from the foundation edge to either side of the domain, as well as the vertical depth of the soil below the foundation. Figure 2 shows the effect of model dimensions on K_V and K_{HH} for a surface foundation on a homogeneous isotropic soil, along with the results of Bell (1991) for a mesh size of $100D$. K_{MH}, K_{MM} and K_T were also investigated and found to be less sensitive to the domain size. It can be seen that a domain size of $50D \sim 100D$ is sufficiently accurate. Thus, a model dimension of $50D$ was adopted for the remaining analyses. The cylindrical circumference of the soil was constrained to prevent out-of-plane translations, and the bottom of the soil was fixed in the three orthogonal coordinate directions (Rahmani et al. 2022; Maleki and Imani 2022), as depicted in Fig. 3.

A mesh convergence study was carried out for a surface foundation on a homogeneous isotropic soil with $\mu = 0.3$, as summarized in Table 1. It is evident that the stiffness coefficients estimated using the medium mesh (185,000 elements) exhibit negligible differences compared to those for the dense mesh (367,000 elements). Therefore, the medium mesh was selected in the analysis. Figure 3 presents a plane view of the three-dimensional model using the medium mesh, which comprised approximately 185,000 eight-node brick elements (i.e. ABAQUS C3D8R) (Dassault Systèmes 2016).

A finer mesh was adopted in the region close to the foundation, gradually transitioning to a coarser mesh in the far field. To capture the stress concentrations

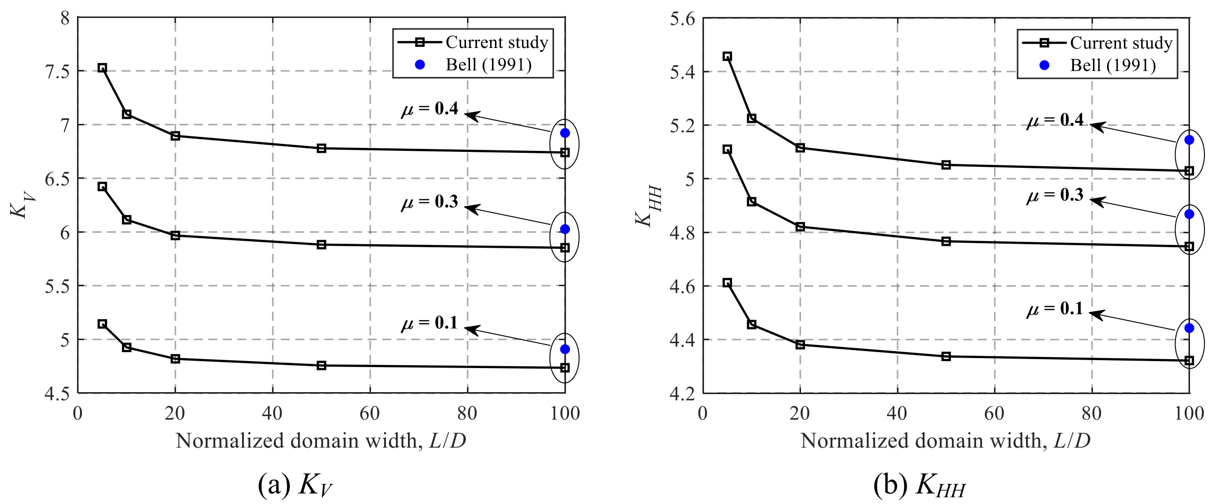

Fig. 2 Effect of model dimensions on the stiffness coefficients for a surface foundation on a homogeneous isotropic soil: **a** K_V and **b** K_{HH}

Fig. 3 Mesh representation

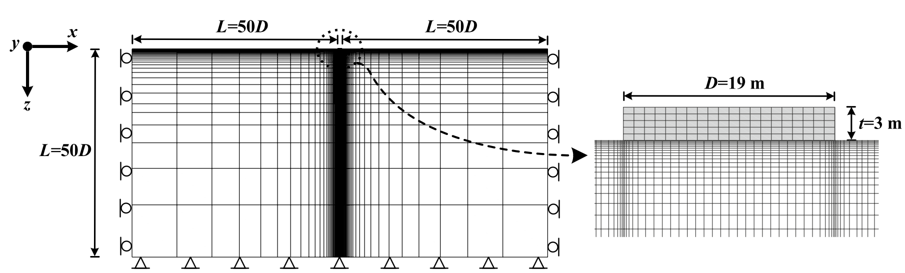

Table 1 Mesh convergence study (surface foundations on a homogeneous soil with $\mu = 0.3$)

Stiffness coefficient	Coarse (35,000 elements)	Medium (185,000 elements)	Dense (367,000 elements)
K_V	5.913	5.924	5.924
K_{HH}	4.787	4.792	4.792
K_{MH}	−0.440	−0.446	−0.446
K_{MM}	3.916	3.966	3.966
K_T	5.251	5.213	5.305

near the foundation edge and the soil-foundation interfaces, the soil regions in the vicinity of the foundation edge and the horizontal thin soil layer close to the interface were carefully refined. For the soil-foundation interfaces in particular, thin layers of soil elements with a thickness of approximately $0.005D$ were employed.

4 Finite element results

4.1 Model calibration

Figure 4 shows the comparison between the stiffness coefficients for a surface circular foundation on a homogeneous isotropic soil obtained from the current FE analysis, the Bell (1991) solutions, and the analytical solutions of Spence (1968), Gerrard and Harrison (1970), Poulos and Davis (1974), and DNV (2016).

The figure shows that the current study compares well (with differences less than 5%) to the solutions of K_V, K_{HH}, K_{MH} and K_{MM} from Bell (1991). Although both of the results are slightly larger than the analytical solutions, the current study lies closer to the analytical solutions than Bell (1991) due to a finer mesh and improved analytical methods. Moreover, the cross-coupling term obtained from Bell (1991) shown in Fig. 4c exhibits good agreement with that derived from the FE analysis. It should also be noted that the current FE results in relatively larger K_{HH} and K_{MM} than the analytical solutions, but the difference between these gradually decreases with increasing μ. This is primarily because the analytical solutions are uncoupled, and the coupling effect gradually decreases with greater μ values, as illustrated in Fig. 4c. Furthermore, Fig. 4c shows no coupling for incompressible soil (i.e. undrained case: of $\mu = 0.5$), making the uncoupled analytical solutions of K_{HH} and K_{MM} approach the current coupled results. As shown in Fig. 4e, the torsional stiffness coefficient given by DNV (2016) remains invariant with μ, being slightly larger than the FE results (with differences less than 1.5%). The agreement observed in Fig. 4 suggests that the current finite element model is expected to remain applicable when altering a single parameter of the model, provided that other model configurations remain unchanged.

4.2 Stiffness coefficient equations for surface foundations on homogeneous soils

The various cases of surface foundations on homogeneous soils can be used to obtain the basic stiffness coefficient equations in the absence of the effects of foundation embedment and soil non-homogeneity. Figure 5a illustrates the variations of K_V with α^2 for different values of μ^*. Generally, K_V gradually increases with the increase of μ^*, but decreases with increasing α^2. This is attributed to the definition of the anisotropy factor as $\alpha^2 = E_h/E_v$, where K_V relies more on the vertical elastic modulus, E_v. To reduce the variability of K_V caused by μ^*, the term $K_V(1.1-\mu^*)$ is introduced, as depicted in Fig. 5b. The figure shows that the FE results (characterized by the range bars showing the mean, lower and upper bounds) fall within a tight band, and a single expression as a function of α^2 is proposed, given by Eq. (15). Figure 5b demonstrates a strong agreement (with $R^2 = 0.997$) between the FE results and the fitted expression.

$$K_V(1.1 - \mu^*) = \frac{3.20 + 3.14\alpha^2}{0.33 + \alpha^2} \tag{15}$$

Equation (15) can be simply manipulated to yield the basic vertical stiffness coefficient equation as:

$$K_V = \left(\frac{1}{1.1 - \mu^*}\right)\left(\frac{3.20 + 3.14\alpha^2}{0.33 + \alpha^2}\right) \tag{16}$$

Isotropy (i.e. $\alpha^2 = 1.0$) simplifies Eq. (16) to the commonly-used isotropic stiffness coefficient (see Eq. (1)).

Similarly, K_{HH} and K_{MM} can be derived in the same way, as seen in Eqs. (17) and (18). The comparison presented in Fig. 6 also shows satisfactory fits between the FE results and the proposed expressions. It is worth noting that K_{MM} decreases with increase of α^2, but K_{HH} shows an opposite trend. This is because K_{MM} is

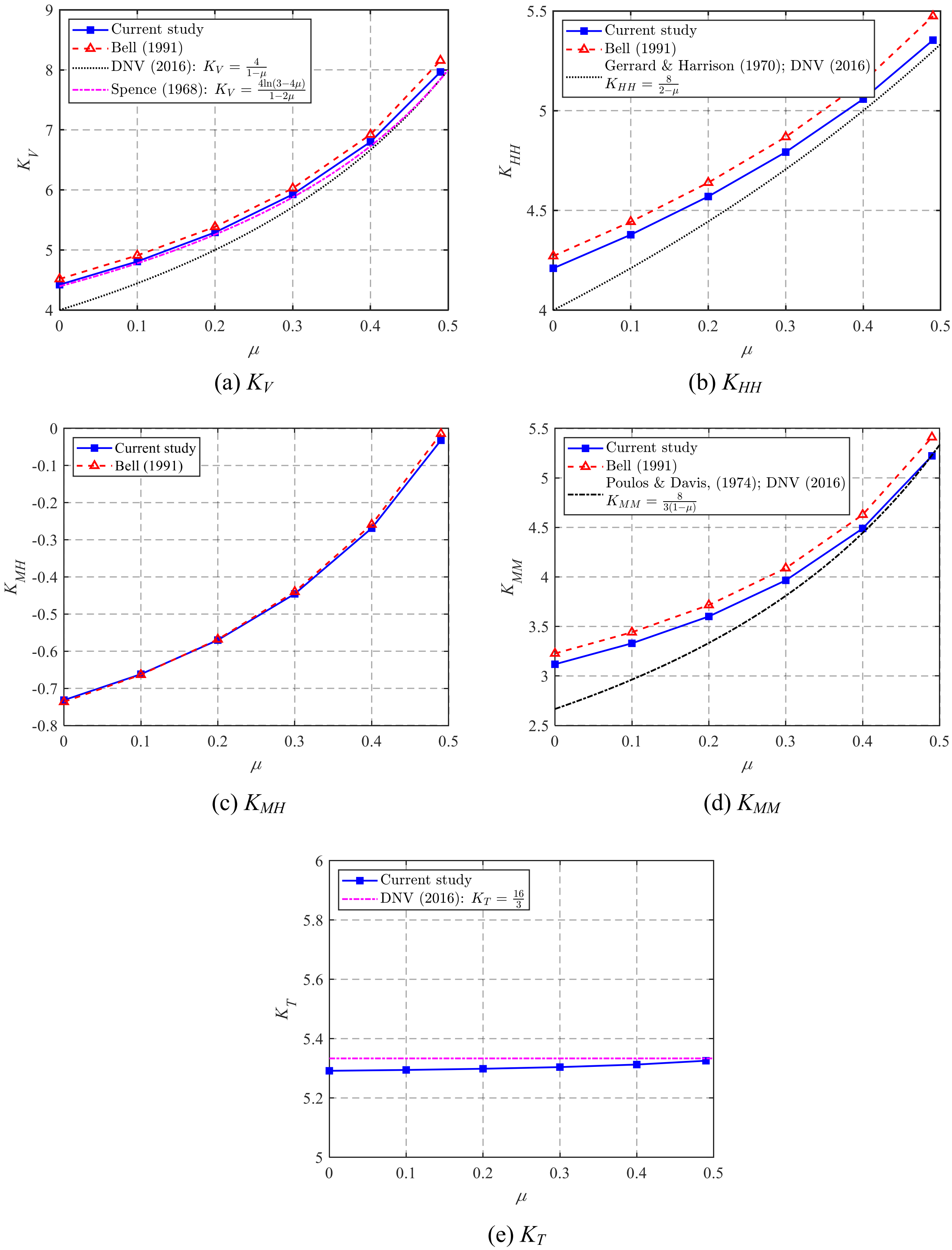

Fig. 4 Stiffness coefficients for a surface circular foundation on a homogeneous isotropic soil: **a** K_V; **b** K_{HH}; **c** K_{MH}; **d** K_{MM} and **e** K_T

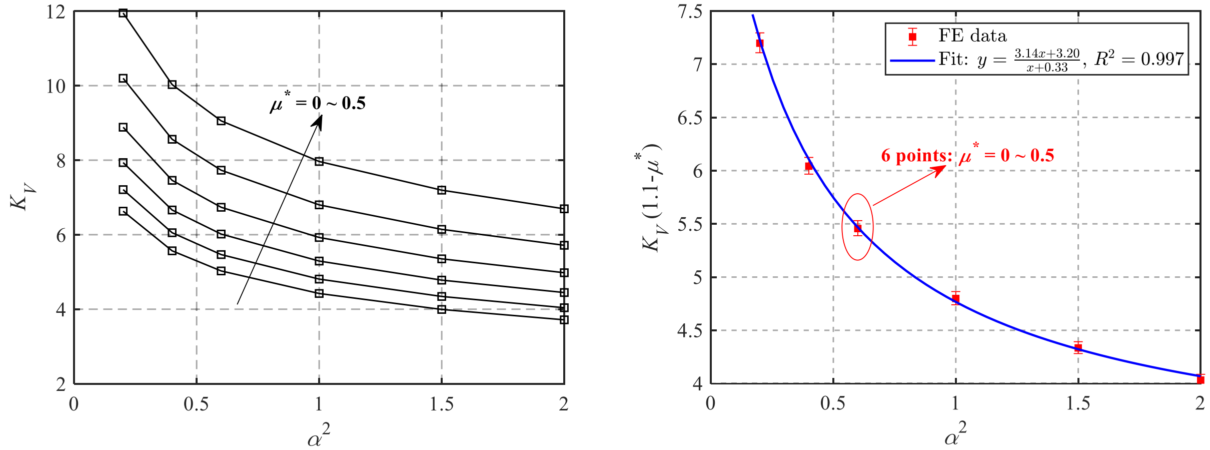

(a) $K_V \sim \alpha^2$ (b) $K_V(1.1–\mu^*) \sim \alpha^2$

Fig. 5 Vertical stiffness coefficient for surface foundations on homogeneous soils: (a) $K_V \sim \alpha^2$ and (b) $K_V\,(1.1-\mu^*) \sim \alpha^2$

dominated by the vertical elastic modulus, while K_{HH} is more influenced by the horizontal elastic modulus.

$$K_{HH} = \left(\frac{1}{2.4 - \mu^*}\right)\left(\frac{6.07 + 15.85\alpha^2}{1.16 + \alpha^2}\right) \tag{17}$$

$$K_{MM} = \left(\frac{1}{1.2 - \mu^*}\right)\left(\frac{2.43 + 2.40\alpha^2}{0.34 + \alpha^2}\right) \tag{18}$$

Figure 7a presents the coupling stiffness coefficient K_{MH} for surface foundations on homogeneous soils. Unlike K_V, K_{HH}, and K_{MM}, K_{MH} appears to be unaffected by the soil anisotropy. Therefore, K_{MH} is simply expressed as a function of μ^*:

$$K_{MH} = K_{HM} = \frac{-1.28(0.5 - \mu^*)}{0.87 - \mu^*} \tag{19}$$

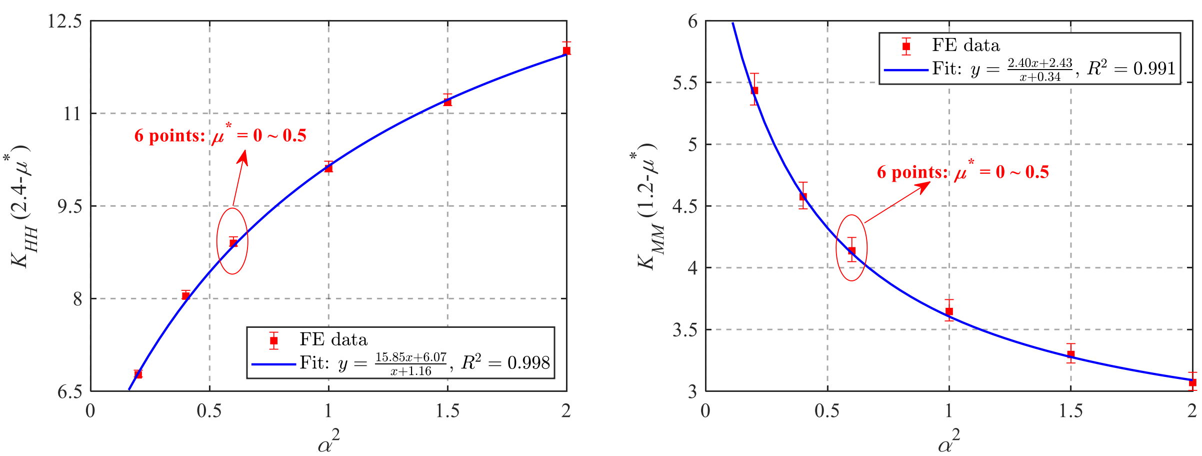

(a) $K_{HH}(2.4–\mu^*)\sim\alpha^2$ (b) $K_{MM}(1.2–\mu^*)\sim\alpha^2$

Fig. 6 Horizontal and rotational stiffness coefficients for surface foundations on homogeneous soils: **a** $K_{HH}(2.4-\mu^*) \sim \alpha^2$ and **b** $K_{MM}(1.2-\mu^*) \sim \alpha^2$

Note that Eq. (19) becomes zero at $\mu^*=0.5$, indicating no coupling effect between horizontal and moment responses. This has also been confirmed by Bell (1991).

The relationship between K_T and α^2 is presented in Fig. 7b. Contrary to K_{MH} shown in Fig. 7a, K_T is affected only by α^2, with μ^* having no influence on K_T. Thus, the relationship is approximated using Eq. (20), and a strong agreement can be observed in Fig. 7b.

$$K_T = \frac{3.20 + 8.33\alpha^2}{1.16 + \alpha^2} \tag{20}$$

4.3 Correction factors for Gibson soils

Analyses of surface shallow foundations on Gibson soils can account for the effects of soil stiffness non-homogeneity on the foundation stiffness. As shown in Eq. (21), a Gibson correction factor for K_V, defined as the ratio of K_V for a Gibson soil to that for a homogeneous soil, is introduced. ($C_{\beta,V}$–1) is adopted to ensure that ($C_{\beta,V}$–1) ~ β curves originate from the origin, as depicted in Fig. 8a. The data points within the ellipse in Fig. 8a represent a single case with the same stiffness slope, including 36 points (six values of α^2 × six values of μ^*). These variations arise due to the dependence of ($C_{\beta,V}$–1) on α^2 and μ^*. Thus, ($C_{\beta,V}$–1) should be expressed as a function of α^2, μ^*, and β, which is simply assumed to be the product of three independent functions in terms of α^2, μ^* and β, respectively:

$$C_{\beta,V} = \frac{K_{V,\,\text{Gibson}}}{K_{V,\,\text{homo}}} = 1 + f_{1,V}(\mu^*) f_{2,V}\left(\alpha^2\right) f_{3,V}(\beta) \tag{21}$$

By using:

$$\begin{aligned} f_{1,V}(\mu^*) &= \tfrac{0.23(1-\mu^*)}{0.77-\mu^*} \\ f_{2,V}\left(\alpha^2\right) &= \tfrac{0.67+0.74\alpha^2}{0.41+\alpha^2} \end{aligned} \tag{22}$$

the relationship between $\frac{C_{\beta,V}-1}{f_{1,V}(\mu^*) f_{2,V}(\alpha^2)}$ and β is shown in Fig. 8. It is evident that the dependence on α^2 and μ^* has been eliminated by dividing $f_{1,V}(\mu^*)$ and $f_{2,V}\left(\alpha^2\right)$, leaving only $f_{3,V}(\beta)$, which is satisfactorily fitted with Eq. (23), as presented in Fig. 8b.

$$f_{3,V}(\beta) = \frac{2.99\beta}{0.81 + \beta} \tag{23}$$

Consequently, $C_{\beta,V}$ can be expressed using Eq. (24).

$$C_{\beta,V} = 1 + \left(\frac{0.23(1-\mu^*)}{0.77-\mu^*}\right)\left(\frac{0.67+0.74\alpha^2}{0.41+\alpha^2}\right)\left(\frac{2.99\beta}{0.81+\beta}\right) \tag{24}$$

Similarly, the Gibson correction factors for K_{HH}, K_{MM} and K_T, are shown in Eqs. (25), (26) and (27),

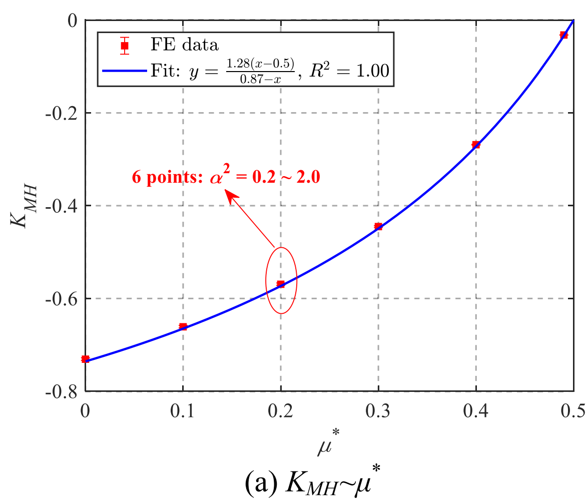

Fig. 7 Coupling and torsional stiffness coefficients for surface foundations on homogeneous soils: **a** K_{MH} ~ μ^* and **b** K_T ~ α^2

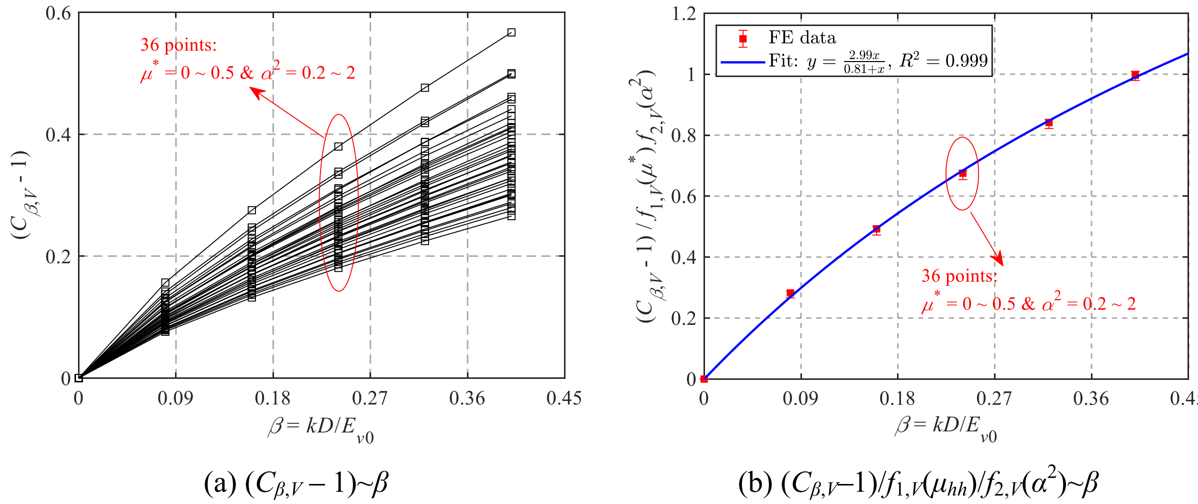

Fig. 8 Gibson correction factor for K_V: **a** $(C_{\beta,V}-1) \sim \beta$ and **b** $(C_{\beta,V}-1)/f_{1,V}(\mu^*)/f_{2,V}(\alpha^2) \sim \beta$

respectively. The comparison presented in Fig. 9 demonstrates an excellent agreement.

$$C_{\beta,HH} = 1 + \left(0.17 - 0.013\mu^*\right)\left(\frac{0.67 + 0.72\alpha^2}{0.41 + \alpha^2}\right)\left(\frac{3.30\beta}{0.93 + \beta}\right) \tag{25}$$

$$C_{\beta,MM} = 1 + \left(\frac{0.062 - 0.056\mu^*}{0.76 - \mu^*}\right)\left(\frac{0.68\left(1 + \alpha^2\right)}{0.37 + \alpha^2}\right)\left(\frac{11.10\beta}{4.03 + \beta}\right) \tag{26}$$

$$C_{\beta,T} = 1 + \left(\frac{0.030\left(1 + \alpha^2\right)}{0.35 + \alpha^2}\right)(2.54\beta) \tag{27}$$

In contrast, the coupling stiffness coefficient K_{MH} seems to be almost unaffected by the soil stiffness non-homogeneity, as illustrated in Fig. 10. Therefore, the Gibson correction factor for K_{MH} is equivalent to 1.0, and the basic equation of K_{MH} for homogeneous soils (see Eq. (19)) is still applicable for Gibson soils, as compared in Fig. 10. Although the variation in K_{MH} at $\mu^* = 0.5$ is relatively larger, the fitted value of $K_{MH} = 0$ at $\mu^* = 0.5$ is still close to the mean value.

4.4 Correction factors for foundation embedment

The effect of foundation embedment on the foundation stiffness is examined using cases of embedded circular foundations in homogeneous soils. Since the influence of the foundation thickness is negligible compared to that of the foundation embedment in this study, particularly for $d/D < 0.5$ (Doherty and Deeks 2003), the foundation embedment depth does not exceed the foundation thickness (i.e. $d \leq t = 3$ m) and the range of the foundation embedment ratio is $d/D \leq 0.16$. Therefore, the effect of the foundation thickness can be ignored and only the effect of foundation embedment is shown in this section.

Similar to the definition of the Gibson correction factors, the embedment correction factor for K_V is also introduced, defined as the ratio of K_V for an embedded foundation in a homogeneous soil to that for a surface foundation on a homogeneous soil. Figure 11a shows the variations of $(C_{d,V}-1)$ with the embedment ratio, d/D. It is evident that for a given value of d/D, a dispersion of the FE results is observed due to the dependence on α^2 and μ^*. Similar $C_{\beta,V}$, $C_{d,V}$ is assumed to follow the same form of equation:

$$C_{d,V} = \frac{K_{V,\text{ emb}}}{K_{V,\text{ surf}}} = 1 + g_{1,V}(\mu^*) g_{2,V}\left(\alpha^2\right) g_{3,V}(d/D) \tag{28}$$

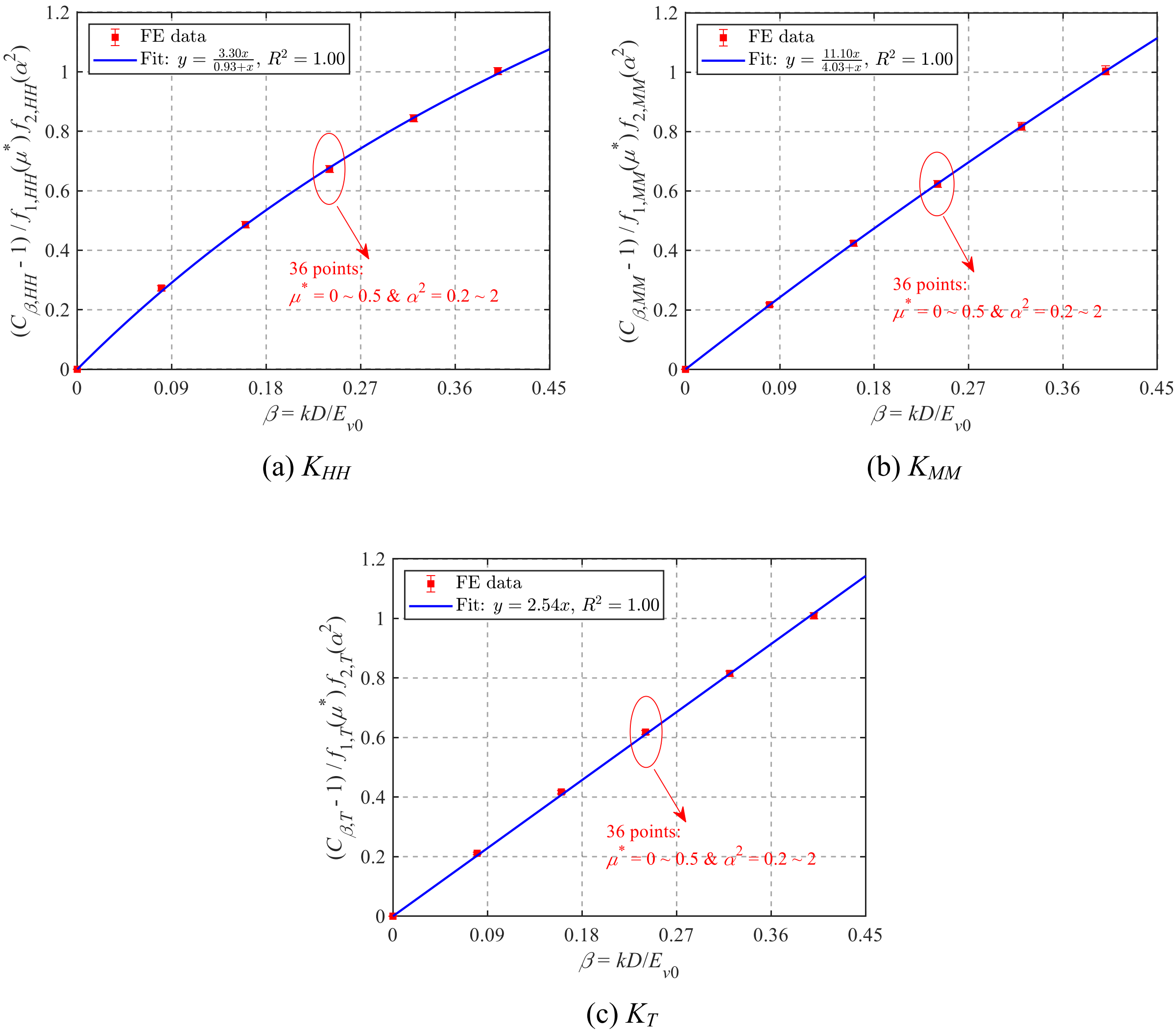

Fig. 9 Gibson correction factors for **a** K_{HH}; **b** K_{MM} and **c** K_T

As shown in Fig. 11b, using $g_{1,V}(\mu^*) = \frac{1.28-1.66\mu^*}{7.45+\mu^*}$ and $g_{2,V}(\alpha^2) = \frac{0.59+1.35\alpha^2}{0.94+\alpha^2}$ results in the FE results falling within a relatively narrow band. The remaining function, $g_{3,V}(d/D)$, can then be approximated using $g_{3,V}(d/D) = \frac{2.61d/D}{0.26+d/D}$, which yields the embedment correction factor for K_V:

$$C_{d,V} = 1 + \left(\frac{1.28 - 1.66\mu^*}{7.45 + \mu^*}\right)\left(\frac{0.59 + 1.35\alpha^2}{0.94 + \alpha^2}\right)\left(\frac{2.61d/D}{0.26 + d/D}\right) \tag{29}$$

Similarly, the embedment correction factors for K_{HH}, K_{MM} and K_T can be developed, as given by Eqs. (30), (31) and (32). A satisfactory comparison can be observed in Fig. 12.

$$C_{d,HH} = 1 + \left(\frac{0.23 - 0.36\mu^*}{0.64 - \mu^*}\right)\left(\frac{0.60 + 1.37\alpha^2}{1.00 + \alpha^2}\right)\left(\frac{2.95d/D}{0.32 + d/D}\right) \tag{30}$$

$$C_{d,MM} = 1 + (0.40 - 0.34\mu^*)\left(\frac{0.71 + 1.60\alpha^2}{1.32 + \alpha^2}\right)\left(\frac{7.56d/D}{1.04 + d/D}\right) \tag{31}$$

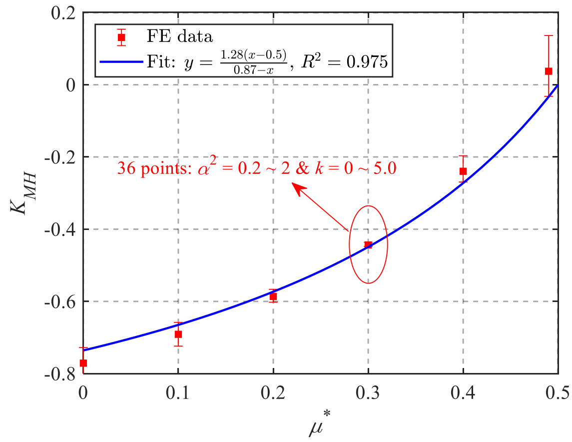

Fig. 10 Coupling stiffness coefficient for surface foundations on Gibson soils

$$C_{d,T} = 1 + \left(\frac{0.20 - 0.27\mu^*}{0.74 - \mu^*}\right)\left(\frac{0.44 + 1.15\alpha^2}{0.55 + \alpha^2}\right)\left(\frac{1.42d/D}{0.068 + d/D}\right) \quad (32)$$

Figure 13a presents the relationship between K_{MH} and d/D. Unlike the effect of Gibson soils, foundation embedment exhibits a significant influence on the coupling stiffness coefficient. Generally, the coupling gradually increases with d/D, aligning with the numerical findings of Bell (1991). As seen in Fig. 13a, six clusters of curves, corresponding to the six values of μ^*, are clearly observed. Note also that K_{MH} at $d/D = 0$ (i.e. surface foundation) is affected only by μ^*. However, with increasing d/D, the effect of α^2 on K_{MH} gradually becomes more pronounced. Therefore, K_{MH} for embedded foundations should be expressed as a function of α^2, μ^*, and β.

Since some values of K_{MH} are close to zero, defining the embedment correction factor for K_{MH} using ratios may lead to singularity. Therefore, the embedment correction factor for K_{MH} is defined using the difference between K_{MH} for an embedded foundation in a homogeneous soil and that for a surface foundation on a homogeneous soil. It is also assumed to be the product of three independent functions of α^2, μ^*, and β, respectively, as expressed by Eq. (33).

$$\begin{aligned} C_{d,MH} = C_{d,HM} &= K_{MH,\,\mathrm{emb}} - K_{MH,\,\mathrm{surf}} \\ &= g_{1,MH}(\mu^*)g_{2,MH}\left(\alpha^2\right)g_{3,MH}(d/D) \end{aligned} \quad (33)$$

Using $g_{1,MH}(\mu^*) = \frac{0.63-0.85\mu^*}{\mu^{*2}-1.97\mu^*+1.21}$ and $g_{2,MH}\left(\alpha^2\right) = \frac{0.75+1.77\alpha^2}{1.51+\alpha^2}$, the remaining function, $g_{3,MH}(d/D) = \frac{C_{d,MH}}{g_{1,MH}(\mu^*)g_{2,MH}(\alpha^2)}$ can be fitted by a linear equation, $g_{3,MH}(d/D) = 6.27d/D$, as favorably compared in Fig. 13b.

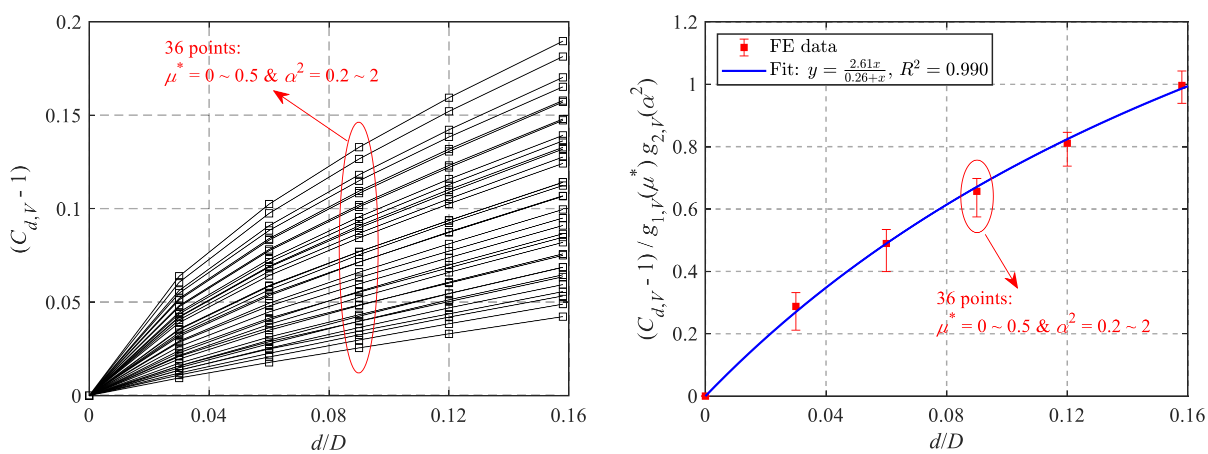

(a) $(C_{d,V}-1) \sim d/D$ (b) $(C_{d,V}-1)/g_{1,V}(\mu^*)/g_{2,V}(\alpha^2) \sim d/D$

Fig. 11 Embedment correction factor for K_V: **a** $(C_{d,V}-1) \sim d/D$ and **b** $(C_{d,V}-1)/g_{1,V}(\mu^*)/g_{2,V}(\alpha^2) \sim d/D$

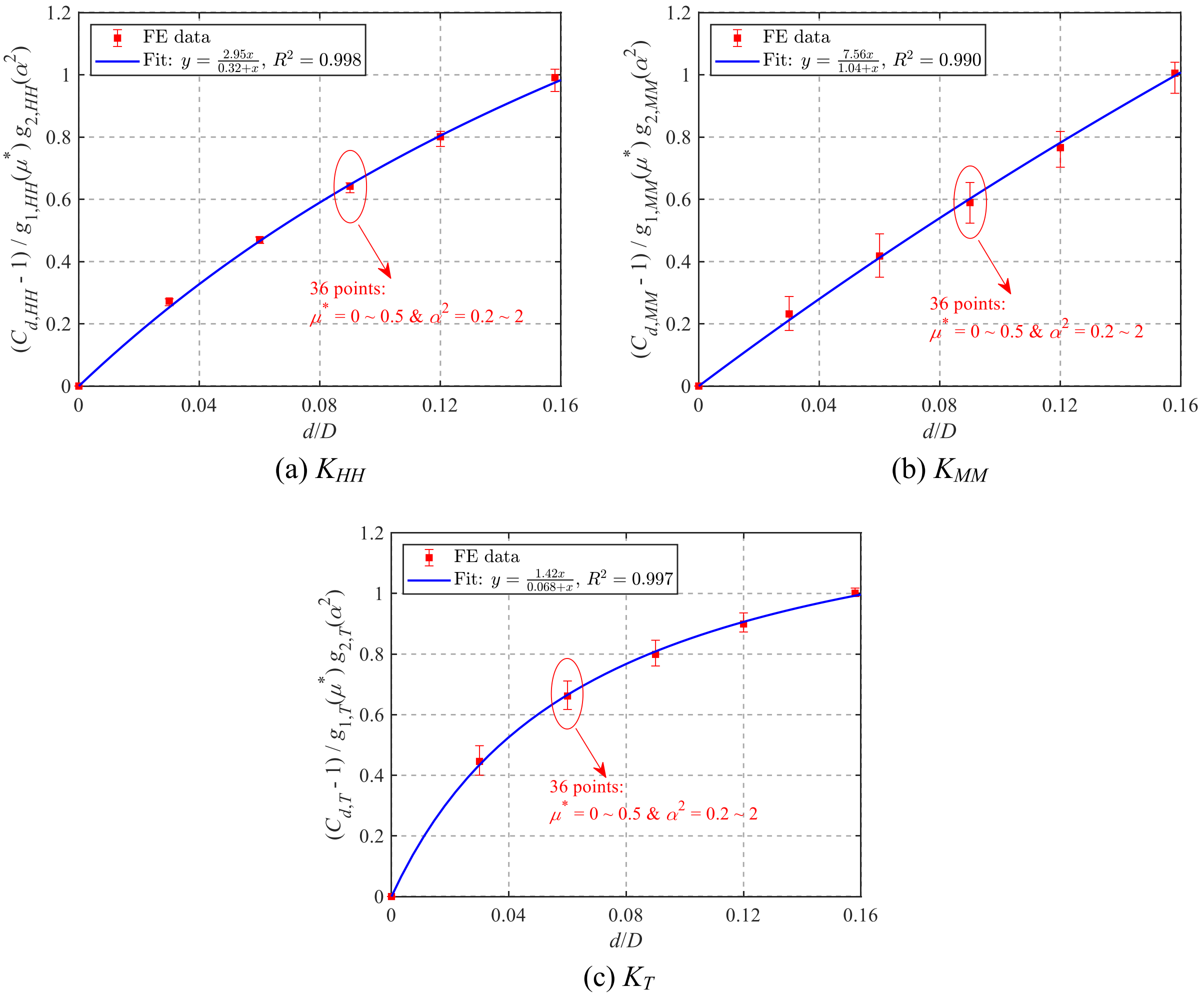

Fig. 12 Embedment correction factors for **a** K_{HH}; **b** K_{MM} and **c** K_T

$$C_{d,MH} = C_{d,HM} = \left(\frac{0.63 - 0.85\mu^*}{\mu^{*2} - 1.97\mu^* + 1.21}\right)\left(\frac{0.75 + 1.77\alpha^2}{1.51 + \alpha^2}\right)(6.27d/D) \tag{34}$$

5 Application

In this section, a typical shallow foundation located on North America wind farm site is examined using the proposed stiffness coefficients, along with the expressions of DNV (2016), Bell (1991), and Gazetas (1991). The coupled coefficient K_{HM} provided by Gazetas (1991) is linearly proportional to d/D and reduces to $K_{HM}=0$ at $d/D=0$, aligning with the stiffness coefficient recommended by DNV (2016).

The complete foundation stiffness coefficients for circular foundations, including both Gibson and embedment correction factors, are summarized in Eq. (35). The properties of the circular foundation and the cross-anisotropic soil are summarized in Table 2, representing typical soil parameters from a glacial clay till deposit situated in Southern Ontario. These clay deposits are typically characterized to be

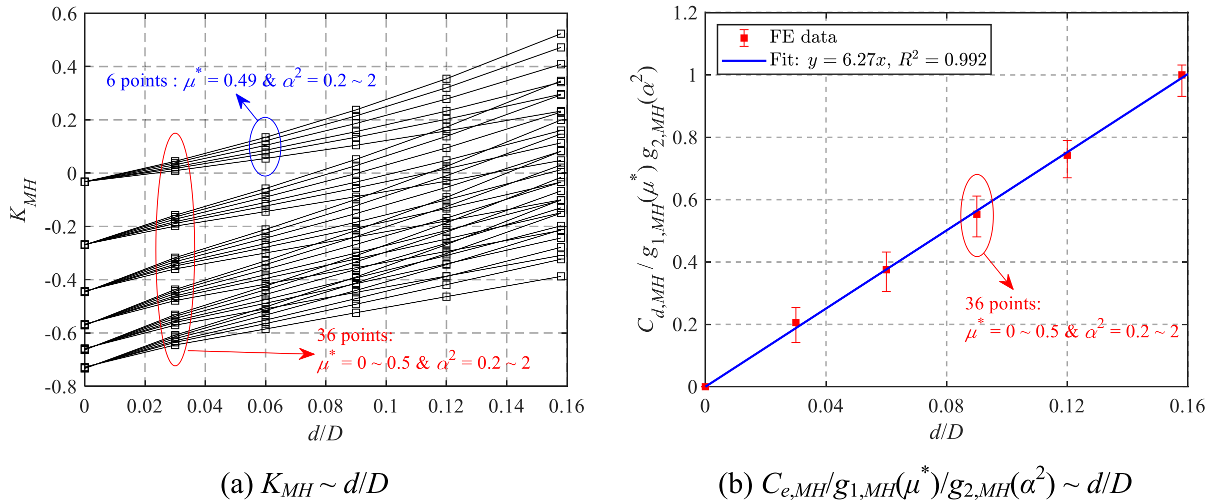

Fig. 13 Embedment correction factor for K_{MH}: **a** $K_{MH} \sim d/D$ and **b** $C_{d,MH}/g_{1,MH}(\mu^*)/g_{2,MH}(\alpha^2) \sim d/D$

Table 2 Foundation and soil parameters

α^2	μ_{hh}	G_{max} at depth of R, [MPa]	k, [MPa/m]	D, [m]	d/D
1.30	0.24	82.0	2	19	0 and 0.16

over-consolidated, stiff, and primarily incompressible with a relatively low moisture content.

Both surface and embedded foundations were considered in the analysis. The factored design loads for the foundation were $V = 21{,}820$ kN, $H = 900$ kN, $M = 60{,}000$ kN·m, and $T = 7{,}300$ kN·m. Note that the shear modulus was taken at a depth equal to the foundation radius (i.e. $G_{hv} = G_R$), following the recommendations of Whitman (1976) and DNV (1992).

$$K_V = \left[\left(\frac{1}{1.1-\mu^*}\right)\left(\frac{3.20+3.14\alpha^2}{0.33+\alpha^2}\right)\right]\left[1+\left(\frac{0.23(1-\mu^*)}{0.77-\mu^*}\right)\left(\frac{0.67+0.74\alpha^2}{0.41+\alpha^2}\right)\left(\frac{2.99\beta}{0.81+\beta}\right)\right]\left[1+\left(\frac{1.28-1.66\mu^*}{7.45+\mu^*}\right)\left(\frac{0.59+1.35\alpha^2}{0.94+\alpha^2}\right)\left(\frac{2.61d/D}{0.26+d/D}\right)\right] \tag{35a}$$

$$K_{HH} = \left[\left(\frac{1}{2.4-\mu^*}\right)\left(\frac{6.07+15.85\alpha^2}{1.16+\alpha^2}\right)\right]\left[1+(0.17-0.013\mu^*)\left(\frac{0.67+0.72\alpha^2}{0.41+\alpha^2}\right)\left(\frac{3.30\beta}{0.93+\beta}\right)\right]\left[1+\left(\frac{0.23-0.36\mu^*}{0.64-\mu^*}\right)\left(\frac{0.60+1.37\alpha^2}{1.00+\alpha^2}\right)\left(\frac{2.95d/D}{0.32+d/D}\right)\right] \tag{35b}$$

$$K_{MH} = K_{HM} = \left[\frac{-1.28(0.5-\mu^*)}{0.87-\mu^*}\right] + \left[\left(\frac{0.63-0.85\mu^*}{\mu^{*2}-1.97\mu^*+1.21}\right)\left(\frac{0.75+1.77\alpha^2}{1.51+\alpha^2}\right)(6.27d/D)\right] \tag{35c}$$

$$K_{MM} = \left[\left(\frac{1}{1.2-\mu^*}\right)\left(\frac{2.43+2.40\alpha^2}{0.34+\alpha^2}\right)\right]\left[1+\left(\frac{0.062-0.056\mu^*}{0.76-\mu^*}\right)\left(\frac{0.68(1+\alpha^2)}{0.37+\alpha^2}\right)\left(\frac{11.10\beta}{4.03+\beta}\right)\right]\left[1+(0.40-0.34\mu^*)\left(\frac{0.71+1.60\alpha^2}{1.32+\alpha^2}\right)\left(\frac{7.56d/D}{1.04+d/D}\right)\right] \tag{35d}$$

$$K_T = \left[\frac{3.20+8.33\alpha^2}{1.16+\alpha^2}\right]\left[1+\left(\frac{0.030(1+\alpha^2)}{0.35+\alpha^2}\right)(2.54\beta)\right]\left[1+\left(\frac{0.20-0.27\mu^*}{0.74-\mu^*}\right)\left(\frac{0.44+1.15\alpha^2}{0.55+\alpha^2}\right)\left(\frac{1.42d/D}{0.068+d/D}\right)\right] \tag{35e}$$

In the absence of other information, DNV (2016) suggests working values of shear strain for a wind turbine foundation of 10^{-3} to estimate soil stiffness reduction, corresponding to approximately $G_R/G_{\max}=0.3$. To assess the site-specific working value of G more accurately, the factored design loads were applied to the FE model in this study, to iteratively calculate the equivalent shear strain (Shrivastava et al. 2012) and the corresponding G_R of at the depth of R using the appropriate shear modulus degradation curve (González-Hurtado 2019). This procedure yields $G_R/G_{\max}=0.43$ at a depth of R.

The foundation responses are compiled in Table 3. It is evident that the vertical settlements u_V calculated by DNV (2016), Bell (1991), and Gazetas (1991) are considerably larger than that obtained in the current study. Regarding the horizontal translation u_H for the surface foundation considering soil anisotropy, the method of Bell (1991) overestimates it, while those methods in DNV (2016) and Gazetas (1991) significantly underestimate it (around 31% of the current value), due to neglecting the coupling effect between horizontal and rotational responses.

For the embedded foundation, the DNV (2016) method provides notably larger u_H compared to the current anlysis, whereas the Gazetas (1991) method considerably underestimates it. In addition, the rocking and torsional angles for the surface foundation estimated by the current study are smaller than those from the other methods. Furthermore, foundation embedment significantly reduces foundation responses, and the rocking angle for the embedded foundation closely aligns with the estimations from the DNV (2016) and Gazetas (1991) methods.

6 Conclusions and recommendations

The coupled elastic stiffness coefficients of circular foundations founded on cross-anisotropic soils under combined VHMT loading were investigated using finite element analysis. A three-parameter cross-anisotropic soil model was adopted with a range of anisotropic parameters covering typical soils found in practice. The findings revealed a decrease in vertical and rocking stiffness coefficients with the anisotropic parameter α, but the horizontal stiffness coefficient exhibits an opposite trend. In addition, the coupling stiffness coefficient remains unaffected by α. To address the effects of soil non-homogeneity and foundation embedment, Gibson soils and embedded foundations were examined separately, and the Gibson and embedment correction factors were derived accordingly. The analysis indicates that a higher Gibson modulus (β) can increase the vertical, horizontal, and moment stiffness coefficients, whilst leaving the coupling between horizontal and moment responses for surface foundations unaffected.

A practical application of the new method was presented to show the effects of soil stiffness anisotropy and foundation embedment on the foundation responses. It was shown that the effects of soil stiffness anisotropy on foundation responses can be significant and should not be ignored. In practical design applications, the soil Gibson factor and anisotropy factor can be determined from laboratory testing (e.g. Kallioglou et al. 2009; González-Hurtado 2019), and Eq. (35) can be applied to calculate the required stiffness coefficients. Given that the design of wind turbine foundations is typically governed by serviceability limit states, a more accurate estimate of foundation stiffnesses, accounting for the collective effects of soil stiffness anisotropy, non-homogeneity, and

Table 3 Foundation responses for $G_R/G_{\max}=0.43$

Response		Current study	DNV (2016)	Bell (1991)	Gazetas (1991)
u_V	$d/D=0$	8.818 (mm)	+40.36%	+31.49%	+40.36%
	$d/D=0.16$	7.878 (mm)	+35.43%	–	+33.59%
u_H	$d/D=0$	0.858 (mm)	−31.12%	+31.24%	−31.12%
	$d/D=0.16$	0.299 (mm)	+62.93%	–	−66.73%
θ_M	$d/D=0$	2.907×10^{-2} (deg.)	+11.49%	+4.77%	+11.49%
	$d/D=0.16$	2.114×10^{-2} (deg.)	−6.52%	–	−6.84%
θ_T	$d/D=0$	0.227×10^{-2} (deg.)	+14.28%	–	+14.28%
	$d/D=0.16$	0.177×10^{-2} (deg.)	−20.92%	–	−20.97%

foundation embedment, can provide more reliable and economical foundation designs.

It is worth noting that the current analysis considered a simplified three-parameter cross-anisotropic elastic model (Graham and Houlsby 1983), rather than a more general cross-anisotropic model, which is left as a refinement for future research. In addition, the analysis focused on embedded foundations at relatively shallow depths ($d/D \leq 0.16$) within the context of large onshore wind turbines. However, with the current trend of increasing wind turbine tower and blade sizes, their foundations will likely require deeper embedments to withstand greater wind loads and moments. Therefore, further work would be valuable to extend the present work to accommodate deeper foundation embedments.

Acknowledgements The authors would like to acknowledge the financial support of Natural Sciences and Engineering Research Council of Canada (Grant No.: RGPIN-2015-06062).

Author contributions All authors contributed to the study conception and design. Numerical model and data analysis were performed by Pengpeng He and Jesús González-Hurtado. The first draft of the manuscript was written by Pengpeng He and all authors commented on previous versions of the manuscript. All authors read and approved the final manuscript.

Funding This work was supported by Natural Sciences and Engineering Research Council of Canada (Grant number: [RGPIN-2015-06062]).

Data availability The datasets generated during the current study are available from the corresponding author on reasonable request.

Declarations

Competing interests The authors have no relevant financial or non-financial interests to disclose.

References

Bell RW (1991) The analysis of offshore foundations subjected to combined loading. Dissertation, University of Oxford

Buragadda V, Orekanti ER (2023) Predicting the allowable settlement of reinforced soil foundations: a laboratory study. Geotech Geol Eng 42:2271–2291. https://doi.org/10.1007/s10706-023-02637-9

Burland JB, Broms BB, De Mello VFB (1977) Behaviour of foundations and structures. In: Proceedings of 9th International conference on soil mechanics and foundation engineering, Tokyo, Japan, 10–15 July 1977. The Japanese Geotechnical Society, Tokyo, Vol. 2, pp 495–546

DNV GL (Det Norske Veritas GL) (1992) Foundations, Classification Notes No. 30.4. DNV GL Group, Høvik, Norway

DNV GL (Det Norske Veritas GL) (2016) DNVGL-ST-0126: Support structures for wind turbines. DNV GL Group, Høvik, Norway

Doherty JP, Deeks AJ (2003) Elastic response of circular footings embedded in a non-homogeneous half-space. Géotechnique 53(8):703–714. https://doi.org/10.1680/geot.2003.53.8.703

Franzius JN (2003) Behaviour of buildings due to tunnel induced subsidence. Dissertation, Imperial College of Science

Gazetas G (1981) Strip foundations on a cross-anisotropic soil layer subjected to dynamic loading. Géotechnique 31(2):161–179. https://doi.org/10.1680/geot.1981.31.2.161

Gazetas G (1991) Formulas and charts for impedances of surface and embedded foundations. J Geotech Eng 117(9):1363–1381. https://doi.org/10.1061/(ASCE)0733-9410(1991)117:9(1363)

Gerrard CM, Harrison WJ (1970) Circular loads applied to a cross-anisotropic half space. Technical Paper No. 8, CSIRO Australian Division of Applied Geomechanics, Australian Geomechanics Society, St Ives, N.S.W

Gibson RE (1967) Some results concerning displacements and stresses in a non-homogeneous elastic half-space. Géotechnique 17(1):58–67. https://doi.org/10.1680/geot.1967.17.1.58

González-Hurtado J (2019) The effect of stiffness anisotropy of a glacial clay on the behaviour of a shallow wind turbine foundation. Dissertation, The University of Western Ontario

Gourvenec SM, Mana DSK (2011) Undrained vertical bearing capacity factors for shallow foundations. Géotechnique Letters 1(4):101–108. https://doi.org/10.1680/geolett.11.00026

Graham J, Houlsby GT (1983) Anisotropic elasticity of a natural clay. Géotechnique 33(2):165–180. https://doi.org/10.1680/geot.1983.33.2.165

Grammatikopoulou A, Schroeder FC, Gasparre A, Kovacevic N, Germano V (2014) The influence of stiffness anisotropy on the behaviour of a stiff natural clay. Geotech Geol Eng 32:1377–1387. https://doi.org/10.1007/s10706-013-9655-1

ISO (International Standards Organization) (2016) ISO 19901–4: Petroleum and natural gas industries specific requirements for offshore structures—part 4: geotechnical and foundation design considerations, 2nd edition. International Standards Organization, Geneva, Switzerland

Kallioglou P, Tika T, Koninis G, Papadopoulos S, Pitilakis K (2009) Shear modulus and damping ratio of organic soils. Geotech Geol Eng 27:217–235. https://doi.org/10.1007/s10706-008-9224-1

Kausel E, Whitman RV, Morray JP, Elsabee F (1978) The spring method for embedded foundations. Nucl Eng Des 48(2–3):377–392. https://doi.org/10.1016/0029-5493(78)90085-7

Korobova OA, Maksimenko LA, Solovyanova IY (2019) Sequence of calculation of anisotropic soil foundations on deformation. *In* Proceedings of International Conference on Construction, Architecture and Technosphere Safety, Chelyabinsk, Russia, 25–27 September 2019. Vol. 687, No. 4, 044036

Lang PJ (2012) Sensitivity of shallow wind turbine foundation design and soil response to geotechnical variance with construction cost implications. Dissertation, University of Wisconsin-Madison

Lings ML (2001) Drained and undrained anisotropic elastic stiffness parameters. Géotechnique 51(6):555–565. https://doi.org/10.1680/geot.2001.51.6.555

Lings ML, Pennington DS, Nash DFT (2000) Anisotropic stiffness parameters and their measurement in a stiff natural clay. Géotechnique 50(2):109–125. https://doi.org/10.1680/geot.2000.50.2.109

Love AEH (1892) A treatise on the mathematical theory of elasticity. Cambridge University Press, Cambridge

Maleki M, Imani M (2022) Active lateral pressure to rigid retaining walls in the presence of an adjacent rock mass. Arab J Geosci 15(2):152. https://doi.org/10.1007/s12517-022-09454-z

Maleki M, Mir Mohammad Hosseini SM (2022) Assessment of the Pseudo-static seismic behavior in the soil nail walls using numerical analysis. Innov Infrastruct Solut 7(4):262. https://doi.org/10.1007/s41062-022-00861-5

Maleki M, Nabizadeh A (2021) Seismic performance of deep excavation restrained by guardian truss structures system using quasi-static approach. SN Appl Sci 3:1–17. https://doi.org/10.1007/s42452-021-04415-9

Maleki M, Khezri A, Nosrati M, Hosseini SMMM (2023) Seismic amplification factor and dynamic response of soil-nailed walls. Model Earth Syst Environ 9(1):1181–1198. https://doi.org/10.1007/s40808-022-01543-y

Nishimura S (2014) Assessment of anisotropic elastic parameters of saturated clay measured in triaxial apparatus: Appraisal of techniques and derivation procedures. Soils Found 54(3):364–376. https://doi.org/10.1016/j.sandf.2014.04.006

Pickering DJ (1970) Anisotropic elastic parameters for soil. Géotechnique 20(3):271–276. https://doi.org/10.1680/geot.1970.20.3.271

Poulos HG (2023) Analysis of foundation settlement interaction among multiple high-rise buildings. Geotech Geol Eng 41:2815–2831. https://doi.org/10.1007/s10706-023-02429-1

Poulos HG, Davis EH (1974) Elastic solutions for soil and rock mechanics. John Wiley & Sons, Hoboken

Rahmani F, Hosseini SM, Khezri A, Maleki M (2022) Effect of grid-form deep soil mixing on the liquefaction-induced foundation settlement, using numerical approach. Arab J Geosci 15(12):1112. https://doi.org/10.1007/s12517-022-10340-x

Ratananikom W, Likitlersuang S, Yimsiri S (2013) An investigation of anisotropic elastic parameters of Bangkok Clay from vertical and horizontal cut specimens. Geomech Geoeng 8(1):15–27. https://doi.org/10.1080/17486025.2012.726746

Raymond GP (1970) Stresses and displacements in cross-anisotropic soil. Géotechnique 20(4):456–458. https://doi.org/10.1680/geot.1963.13.3.198

Reissner E, Sagoci HF (1944) Forced torsional oscillations of an elastic half-space. I. J Appl Phys 15(9):652–654. https://doi.org/10.1063/1.1707489

Rowe RK, Booker JR (1981) The behaviour of footings resting on a non-homogeneous soil mass with a crust. Part II. Circular footings. Can Geotech J 18(2):265–279. https://doi.org/10.1139/t81-029

Shrivastava S, Ghosh C, Jonas JJ (2012) A comparison of the von Mises and Hencky equivalent strains for use in simple shear experiments. Philos Mag 92(7):779–786. https://doi.org/10.1080/14786435.2011.634848

Simpson B, Atkinson AJ, Jovicic V (1996) The influence of anisotropy on calculations of ground settlements above tunnels. In: Mair RJ, Taylor RN (eds) Geotechnical aspects of underground construction in soft ground. Balkema, Rotterdam, pp 591–594

Singh S, Tanyu BF, Lade PV (2024) Characteristic behavior of cross-anisotropic deposits of granular soils. Geotech Geol Eng 42:61–78. https://doi.org/10.1007/s10706-023-02553-y

Spence DA (1968) Self similar solutions to adhesive contact problems with incremental loading. Proc R Soc Lond A 305(1480):55–80

Systèmes D (2016) Abaqus analysis user's manual. Simulia Corp, USA

Whitman RV (1976) Soil-platform interaction. In Proceedings of conference on behaviour of offshore structures, Oslo, Norway, 1976. Norwegian Institute of Technology, Trondheim, 1, 817

Yimsiri S, Soga K (2011) Cross-anisotropic elastic parameters of two natural stiff clays. Géotechnique 61(9):809–814. https://doi.org/10.1680/geot.9.P.072

Zarei C, Soltani-Jigheh H (2021) Anisotropic behavior of cohesive soils by considering effect of gradation and plasticity characteristics. Geotech Geol Eng 39:2739–2754. https://doi.org/10.1007/s10706-020-01654-2